**DEPARTMENT OF ASTRONOMY, UNIVERSITY OF VIRGINIA**

**TITLE:** **Ideal Magnetohydrodynamics and Its Realization on Cartesian Grids***

**AUTHOR:** Andrew Y. Jiao

**INSTRUCTOR:** Phil Arras

**DATE:** December 6, 2019

**ABSTRACT:** We studied the ideal magnetohydrodynamic (MHD) system by deriving the well known results of the Alfvén and magnetosonic modes characteristic of the system, as well as the Rankine-Hugoniot jump conditions for MHD. An ideal MHD solver was implemented in Julia on a 2D Cartesian grid using the 5th-order WENO finite-difference scheme. Divergence corrections were done by evolving the vector potential alongside the MHD system. The Orszag-Tang vortex was implemented to test shock capturing and the formation of MHD turbulence from smooth initial conditions, while Alfvén wave perturbations were implemented to test grid convergence and to test for agreement with analytical solutions.

*This thesis is submitted in partial completion of the requirements of the Bachelor of Science in Physics.

## 1 Introduction

Magnetohydrodynamics (MHD) is the field of physics which describes the dynamics of fluids under the influence of magnetic fields. MHD can be used to describe astrophysical processes and is a good starting point for modeling plasma instabilities.

MHD physics is contained in the generalized Ohm's law. We define the electron mass $m_e$, ion mass $m_i$, electric charge $e$, speed of light $c$, current density $\mathbf{J}$, mass density $\rho$, flow velocity $\mathbf{u}$, pressure tensor $\mathsf{P}$, electric field $\mathbf{E}$, magnetic field $\mathbf{B}$, and conductivity $\sigma$. Then the generalized Ohm's law reads as

$$\frac{m_e m_i}{\rho e^2}\frac{\partial \mathbf{J}}{\partial t} - \frac{m_i}{\rho e}\boldsymbol{\nabla}\cdot\mathsf{P} = \mathbf{E} + \frac{1}{c}\,\mathbf{u}\times\mathbf{B} - \frac{m_i}{\rho e c}\,\mathbf{J}\times\mathbf{B} - \frac{1}{\sigma}\,\mathbf{J} \tag{1}$$

where the terms are interpreted from left to right as the electron inertia, electron pressure, electric field, convective field, Hall field, and the conductivity.

The electron inertia can be neglected at length scales longer than the electron inertial length and time scales longer than an electron cyclotron period. The conductivity can be neglected for plasmas with very high conductivity, e.g. for many fully ionized plasmas. The Hall and electron pressure terms can be neglected at length scales longer than the ion inertial length and time scales longer than an ion cyclotron period. When all of these are assumed, we are left with ideal MHD, with an electric field of the form

$$\mathbf{E} = -\frac{1}{c}\,\mathbf{u}\times\mathbf{B}. \tag{2}$$

Substituting into Faraday's law yields the induction equation $\partial_t\mathbf{B} = \boldsymbol{\nabla}\times(\mathbf{u}\times\mathbf{B})$, describing the dynamics of the magnetic field. One important property of ideal MHD is that it satisfies Alfvén's theorem of the preservation of magnetic topology – that is, the magnetic field lines are frozen into the bulk fluid. The theorem is written in terms of the change in magnetic flux

$$\frac{\mathrm{d}\Phi_B}{\mathrm{d}t} = \int_S \frac{\partial \mathbf{B}}{\partial t}\cdot\mathrm{d}\mathbf{S} + \oint_{\partial S}\mathbf{B}\cdot(\mathbf{u}\times\mathrm{d}\mathbf{l}) = -c\oint_{\partial S}\left(\mathbf{E}+\frac{1}{c}\,\mathbf{u}\times\mathbf{B}\right)\cdot\mathrm{d}\mathbf{l} = 0$$

where we used Faraday's law, Stokes' theorem, and a scalar triple product identity. The relation (2) means that $\mathbf{E}\perp\mathbf{B}$, so it is not possible in this model for the electric field to accelerate particles.

The ideal MHD equations in conservative form are

$$\frac{\partial}{\partial t}\begin{pmatrix}\rho\\ \rho\mathbf{u}\\ E\\ \mathbf{B}\end{pmatrix} + \boldsymbol{\nabla}\cdot\begin{pmatrix}\rho\mathbf{u}\\ \rho\mathbf{u}\otimes\mathbf{u} + P_{\mathrm{tot}}\mathsf{I} - \frac{1}{4\pi}\,\mathbf{B}\otimes\mathbf{B}\\ \mathbf{u}(E+P_{\mathrm{tot}}) - \frac{1}{4\pi}\,\mathbf{B}(\mathbf{u}\cdot\mathbf{B})\\ \mathbf{u}\otimes\mathbf{B} - \mathbf{B}\otimes\mathbf{u}\end{pmatrix} = 0 \tag{3}$$

along with the divergence constraint $\boldsymbol{\nabla}\cdot\mathbf{B} = 0$. Above, $P$ is the pressure (we assume that $\mathsf{P} = P\mathsf{I}$), $\gamma$ is the adiabatic index, and

$$P_{\mathrm{tot}} = P + \frac{B^2}{8\pi} \quad\text{and}\quad E = \frac{P}{\gamma-1} + \frac{1}{2}\rho u^2 + \frac{B^2}{8\pi}$$

are respectively the total pressure and energy. In the implementation in the code, we take $\gamma = 5/3$.

Ideal MHD can also be derived from the two-fluid equations and describes the physics of a one-fluid plasma in the limit where the ions contain all the mass and the electrons contain all the current. This derivation is readily found in standard plasma physics textbooks.

The ideal MHD system is similar in form to the Euler equations of fluid dynamics, but owing to the presence of the magnetic field, this system is considerably more complicated to describe, with three characteristic waves and speeds, compared to just the sound speed in the Euler system. Even so, it is the simplest system which can describe the physics of plasmas, highlighting the overall difficulty of plasma modeling.

## 2 Linearized equations and MHD waves

In this section, we derive the three waves present in ideal MHD. We start with defining perturbed quantities denoted with the subscript 1, so that $\rho = \rho_0 + \rho_1$, $P = P_0 + P_1$, $\mathbf{B} = \mathbf{B}_0 + \mathbf{B}_1$, $\mathbf{J} = \mathbf{J}_1$ and $\mathbf{u} = \mathbf{u}_1$, where the flow velocity and current density are assumed to be zero in equilibrium, and $\rho_0$, $P_0$, and $\mathbf{B}_0$ are constant, implying that $\boldsymbol{\nabla} \times \mathbf{B}_0 = 0$ and $\boldsymbol{\nabla}\rho_0 = \boldsymbol{\nabla}P_0 = \boldsymbol{\nabla}\mathbf{B}_0 = 0$. Without loss of generality, we can define the magnetic field to be uniform in the $z$ direction: $\mathbf{B}_0 = B_0\hat{\mathbf{z}}$. The linearized equations (in nonconservative form) are then

$$\begin{aligned}
\frac{\partial \rho_1}{\partial t} + \boldsymbol{\nabla} \cdot (\rho_0 \mathbf{u}_1) &= 0 \\
\frac{\partial \mathbf{B}_1}{\partial t} + \boldsymbol{\nabla} \times (\mathbf{B}_0 \times \mathbf{u}_1) &= 0 \\
\frac{\partial P_1}{\partial t} + (\mathbf{u}_1 \cdot \boldsymbol{\nabla}) P_0 + \gamma P_0 \boldsymbol{\nabla} \cdot \mathbf{u}_1 &= 0 \\
\rho_0 \frac{\partial \mathbf{u}_1}{\partial t} + \boldsymbol{\nabla} P_1 - \frac{1}{4\pi}(\boldsymbol{\nabla} \times \mathbf{B}_1) \times \mathbf{B}_0 &= 0.
\end{aligned}$$

Using the perturbed flow velocity $\mathbf{u}_1$, we define a displacement

$$\boldsymbol{\xi} = \int_0^t \mathbf{u}_1(\mathbf{r}, t')\, \mathrm{d}t' \quad \text{such that} \quad \frac{\partial \boldsymbol{\xi}}{\partial t} = \mathbf{u}_1(\mathbf{r}, t).$$

Replacing $\mathbf{u}_1 \to \partial_t \boldsymbol{\xi}$ in the linearized equations and doing some rearranging, we have

$$\begin{aligned}
\frac{\partial \rho_1}{\partial t} &= -\rho_0 \boldsymbol{\nabla} \cdot \frac{\partial \boldsymbol{\xi}}{\partial t} - \frac{\partial \boldsymbol{\xi}}{\partial t} \cdot \boldsymbol{\nabla}\rho_0 \\
\frac{\partial \mathbf{B}_1}{\partial t} &= \boldsymbol{\nabla} \times \left( \frac{\partial \boldsymbol{\xi}}{\partial t} \times \mathbf{B}_0 \right) \\
\frac{\partial P_1}{\partial t} &= -\left( \frac{\partial \boldsymbol{\xi}}{\partial t} \cdot \boldsymbol{\nabla} \right) P_0 - \gamma P_0 \boldsymbol{\nabla} \cdot \frac{\partial \boldsymbol{\xi}}{\partial t} \\
\rho_0 \frac{\partial^2 \boldsymbol{\xi}}{\partial t^2} &= -\boldsymbol{\nabla} P_1 + \frac{1}{4\pi}(\boldsymbol{\nabla} \times \mathbf{B}_1) \times \mathbf{B}_0.
\end{aligned}$$

The last equation contains a second time derivative and hence is the best candidate from which a wave equation may emerge. Integrating and noting that the background mass density, pressure, and magnetic field are all constant, we have $\rho_1 = -\rho_0 \boldsymbol{\nabla} \cdot \boldsymbol{\xi}$, $\mathbf{B}_1 = \boldsymbol{\nabla} \times (\boldsymbol{\xi} \times \mathbf{B}_0)$, and $P_1 = -\gamma P_0 \boldsymbol{\nabla} \cdot \boldsymbol{\xi}$, which we substitute into the momentum equation to obtain

$$\rho_0 \frac{\partial^2 \boldsymbol{\xi}}{\partial t^2} = \boldsymbol{\nabla}((\boldsymbol{\xi} \cdot \boldsymbol{\nabla}) P_0 + \gamma P_0 \boldsymbol{\nabla} \cdot \boldsymbol{\xi}) + \frac{1}{4\pi} \boldsymbol{\nabla} \times (\boldsymbol{\nabla} \times (\boldsymbol{\xi} \times \mathbf{B}_0)) \times \mathbf{B}_0. \tag{4}$$

We assume that the displacement can be decomposed into its Fourier components

$$\boldsymbol{\xi}(\mathbf{r}, t) = \sum_{\mathbf{k}, \omega} \boldsymbol{\xi}(\mathbf{k}, \omega) e^{i(\mathbf{k} \cdot \mathbf{r} - \omega t)},$$

allowing us to make the substitutions $\partial_t \to -i\omega$ and $\boldsymbol{\nabla} \to i\mathbf{k}$. We assume that the wavevector resides in the $yz$-plane and that $\mathbf{k} = (0, k_\perp, k_\parallel)^T$ and $k^2 = k_\perp^2 + k_\parallel^2$, denoting the components of the wavevector perpendicular and parallel to $\mathbf{B}_0$. Using the vector identity $\boldsymbol{\nabla} \times (\mathbf{A} \times \mathbf{B}) = \mathbf{A}(\boldsymbol{\nabla} \cdot \mathbf{B}) - \mathbf{B}(\boldsymbol{\nabla} \cdot \mathbf{A}) + (\mathbf{B} \cdot \boldsymbol{\nabla})\mathbf{A} - (\mathbf{A} \cdot \boldsymbol{\nabla})\mathbf{B}$, we have

$$\rho_0 \omega^2 \boldsymbol{\xi} = \gamma P_0 \mathbf{k}(\mathbf{k} \cdot \boldsymbol{\xi}) + \frac{1}{4\pi}(\mathbf{k} \times ((\mathbf{B}_0 \cdot \mathbf{k})\boldsymbol{\xi} - \mathbf{B}_0(\mathbf{k} \cdot \boldsymbol{\xi}))) \times \mathbf{B}_0.$$

We use the fact that $\mathbf{k} \cdot \boldsymbol{\xi} = k_\perp \xi_y + k_\parallel \xi_z$ and $\mathbf{B}_0 \cdot \mathbf{k} = B_0 k_\parallel$ to simplify the cross products on the right hand side. Writing by components, the equations are

$$\begin{aligned}
\rho_0 \omega^2 \xi_x &= \frac{1}{4\pi} \xi_x k_\parallel^2 B_0^2 \\
\rho_0 \omega^2 \xi_y &= \gamma P_0 k_\perp \left(k_\perp \xi_y + k_\parallel \xi_z\right) + \frac{1}{4\pi} \xi_y B_0^2 k^2 \\
\rho_0 \omega^2 \xi_z &= \gamma P_0 k_\parallel \left(k_\perp \xi_y + k_\parallel \xi_z\right).
\end{aligned}$$

This is an eigenvalue equation, and we want to find nontrivial solutions to the equation

$$\begin{pmatrix}
\frac{B_0^2}{4\pi\rho_0}\frac{k_\parallel^2}{\omega^2} - 1 & 0 & 0 \\
0 & \frac{\gamma P_0}{\rho_0}\frac{k_\perp^2}{\omega^2} + \frac{B_0^2}{4\pi\rho_0}\frac{k^2}{\omega^2} - 1 & \frac{\gamma P_0}{\rho_0}\frac{k_\perp k_\parallel}{\omega^2} \\
0 & \frac{\gamma P_0}{\rho_0}\frac{k_\perp k_\parallel}{\omega^2} & \frac{\gamma P_0}{\rho_0}\frac{k_\parallel^2}{\omega^2} - 1
\end{pmatrix} \boldsymbol{\xi} = 0. \tag{5}$$

From here, we obtain the dispersion equation

$$\left(\frac{B_0^2}{4\pi\rho_0}\frac{k_\parallel^2}{\omega^2} - 1\right)\left[\left(\frac{\gamma P_0}{\rho_0}\frac{k_\perp^2}{\omega^2} + \frac{B_0^2}{4\pi\rho_0}\frac{k^2}{\omega^2} - 1\right)\left(\frac{\gamma P_0}{\rho_0}\frac{k_\parallel^2}{\omega^2} - 1\right) - \left(\frac{\gamma P_0}{\rho_0}\frac{k_\perp k_\parallel}{\omega^2}\right)^2\right] = 0. \tag{6}$$

The first one is the Alfvén wave

$$\frac{B_0^2}{4\pi\rho_0}\frac{k_\parallel^2}{\omega^2} = 1 \quad \to \quad \boxed{\frac{\omega^2}{k_\parallel^2} = \frac{B_0^2}{4\pi\rho_0}.} \tag{7}$$

From (6), we find it convenient to define the Alfvén and sound speeds as $v_A = B_0/\sqrt{4\pi\rho_0}$ and $v_s = \sqrt{\gamma P_0/\rho_0}$. The second and third solutions are obtained with the quadratic in $\omega^2$

$$\omega^4 - \omega^2\left(v_A^2 k^2 + v_s^2 k^2\right) + v_A^2 v_s^2 k_\parallel^2 k^2 = 0 \tag{8}$$

which are the fast and slow magnetosonic waves

$$\boxed{\frac{\omega^2}{k^2} = \frac{1}{2}\left[v_A^2 + v_s^2 \pm \sqrt{\left(v_A^2 + v_s^2\right)^2 - 4v_A^2 v_s^2 \frac{k_\parallel^2}{k^2}}\right].} \tag{9}$$

Alternatively, defining $\theta$ as the angle between $\mathbf{k}$ and $\mathbf{B}_0$, we have that $k_\parallel^2/k^2 = \cos^2\theta$ and $k_\parallel = k\cos\theta$, so the dispersion relations become

$$\frac{\omega^2}{k^2} = v_A^2 \cos^2\theta \qquad \text{(Alfvén)}$$

$$\frac{\omega^2}{k^2} = \frac{1}{2}\left[v_A^2 + v_s^2 \pm \sqrt{\left(v_A^2 + v_s^2\right)^2 - 4v_A^2 v_s^2 \cos^2\theta}\right]. \qquad \text{(Magnetosonic)}$$

The Alfvén wave possesses a wavevector that is parallel to $\mathbf{B}_0$ because only $k_\parallel$ is present in its dispersion relation. Without deriving the exact form of the eigenvectors, we see that the Alfvén wave only has an $x$ component $(\xi_x, 0, 0)^T$, which is trivally found from the matrix, so that with this wave, $\boldsymbol{\xi} \cdot \mathbf{k} = 0$ and $\boldsymbol{\xi} \cdot \mathbf{B}_0 = 0$ – in other words, Alfvén waves are transverse and incompressible.

The fast and slow magnetosonic waves have nonvanishing $y$ and $z$ components $(0, \xi_y, \xi_z)^T$, so that $\boldsymbol{\xi} \cdot \mathbf{k} \neq 0$ and $\boldsymbol{\xi} \cdot \mathbf{B}_0 \neq 0$ – in other words, magnetosonic waves have both a transverse and longitudinal component to them. The eigenvectors are found by ruling out the individual possibilities of $\xi_x \neq 0$, $\xi_y = 0$, and $\xi_z = 0$ in the general scenario ($\sin\theta \cos\theta \neq 0$ for arbitrary $\theta$; equivalently, it is not always true that $k_\perp = 0$ or $k_\parallel = 0$). This also implies that magnetosonic waves are compressible, hence the name.

In the fast and slow wave limits of (8), one obtains the respective dispersions

$$\frac{\omega^2}{k^2} = v_A^2 + v_s^2 \quad \text{and} \quad \frac{\omega^2}{k_\parallel^2} = \frac{v_A^2 v_s^2}{v_A^2 + v_s^2}.$$

The slow wave resembles the dispersion of the Alfvén wave in the limit that $v_s^2 \gg v_A^2$.

## 3 Conservation of energy

Our objective in this section is to obtain a conservation equation for the perturbed energy in the form $\partial_t E_1 + \boldsymbol{\nabla} \cdot \mathbf{F}_{E_1} = 0$. We begin with the momentum equation (4). We assume that $P_0$ and $\mathbf{B}_0$ are constant again, so one of the terms in the gradient can be sent to zero. Hence we have

$$\rho_0 \frac{\partial^2 \boldsymbol{\xi}}{\partial t^2} = \gamma P_0 \boldsymbol{\nabla}(\boldsymbol{\nabla} \cdot \boldsymbol{\xi}) + \frac{1}{4\pi}(\boldsymbol{\nabla} \times \mathbf{B}_1) \times \mathbf{B}_0.$$

We multiply each side by $\mathbf{u}_1$. Then

$$\rho_0 \frac{\partial \boldsymbol{\xi}}{\partial t} \cdot \frac{\partial^2 \boldsymbol{\xi}}{\partial t^2} = \frac{\partial}{\partial t}\left(\frac{1}{2}\rho_0 u_1^2\right) = \gamma P_0 \frac{\partial \boldsymbol{\xi}}{\partial t} \cdot \boldsymbol{\nabla}(\boldsymbol{\nabla} \cdot \boldsymbol{\xi}) + \frac{1}{4\pi}\frac{\partial \boldsymbol{\xi}}{\partial t} \cdot ((\boldsymbol{\nabla} \times \mathbf{B}_1) \times \mathbf{B}_0).$$

The first term is

$$\begin{aligned}
\gamma P_0 \frac{\partial \boldsymbol{\xi}}{\partial t} \cdot \boldsymbol{\nabla}(\boldsymbol{\nabla} \cdot \boldsymbol{\xi}) &= \gamma P_0 \left[\boldsymbol{\nabla} \cdot \left(\frac{\partial \boldsymbol{\xi}}{\partial t}(\boldsymbol{\nabla} \cdot \boldsymbol{\xi})\right) - (\boldsymbol{\nabla} \cdot \boldsymbol{\xi})\left(\boldsymbol{\nabla} \cdot \frac{\partial \boldsymbol{\xi}}{\partial t}\right)\right] \\
&= \gamma P_0 \left[\boldsymbol{\nabla} \cdot \left(\frac{\partial \boldsymbol{\xi}}{\partial t}(\boldsymbol{\nabla} \cdot \boldsymbol{\xi})\right) - \frac{\partial}{\partial t}\left(\frac{1}{2}(\boldsymbol{\nabla} \cdot \boldsymbol{\xi})^2\right)\right] \\
&= -\frac{\partial}{\partial t}\left(\frac{1}{2}\gamma P_0 (\boldsymbol{\nabla} \cdot \boldsymbol{\xi})^2\right) + \boldsymbol{\nabla} \cdot [\gamma P_0 \mathbf{u}_1 (\boldsymbol{\nabla} \cdot \boldsymbol{\xi})].
\end{aligned}$$

The second term is

$$\begin{aligned}
\frac{1}{4\pi}\frac{\partial \boldsymbol{\xi}}{\partial t} \cdot ((\boldsymbol{\nabla} \times \mathbf{B}_1) \times \mathbf{B}_0) &= -\frac{1}{4\pi}(\boldsymbol{\nabla} \times \mathbf{B}_1) \cdot \frac{\partial}{\partial t}(\boldsymbol{\xi} \times \mathbf{B}_0) \\
&= -\frac{1}{4\pi}\left[\boldsymbol{\nabla} \cdot \left(\mathbf{B}_1 \times \frac{\partial}{\partial t}(\boldsymbol{\xi} \times \mathbf{B}_0)\right) + \mathbf{B}_1 \cdot \left(\boldsymbol{\nabla} \times \frac{\partial}{\partial t}(\boldsymbol{\xi} \times \mathbf{B}_0)\right)\right] \\
&= -\frac{1}{4\pi}\left[\boldsymbol{\nabla} \cdot (\mathbf{B}_1 \times (\mathbf{u}_1 \times \mathbf{B}_0)) + \mathbf{B}_1 \cdot \frac{\partial \mathbf{B}_1}{\partial t}\right] \\
&= \boldsymbol{\nabla} \cdot \left[-\frac{1}{4\pi}(\mathbf{u}_1(\mathbf{B}_1 \cdot \mathbf{B}_0) - \mathbf{B}_0(\mathbf{B}_1 \cdot \mathbf{u}_1))\right] - \frac{\partial}{\partial t}\left(\frac{B_1^2}{8\pi}\right).
\end{aligned}$$

Thus the energy equation is

$$\frac{\partial}{\partial t}\left[\frac{1}{2}\rho_0 u_1^2 + \frac{1}{2}\gamma P_0(\boldsymbol{\nabla}\cdot\boldsymbol{\xi})^2 + \frac{B_1^2}{8\pi}\right] + \boldsymbol{\nabla}\cdot\left[-\gamma P_0(\boldsymbol{\nabla}\cdot\boldsymbol{\xi})\mathbf{u}_1 + \frac{1}{4\pi}(\mathbf{u}_1(\mathbf{B}_0\cdot\mathbf{B}_1) - \mathbf{B}_0(\mathbf{u}_1\cdot\mathbf{B}_1))\right] = 0. \tag{10}$$

The perturbed energy density takes on a similar form to the energy density in the full nonlinear equation, with the exception of the pressure term that relies on the compression $\boldsymbol{\nabla}\cdot\boldsymbol{\xi}$.

## 4 Shocks

We begin with an MHD shock and decompose the dynamic variables to components parallel and perpendicular to the shock front. We denote derivatives with respect to $s$ and $n$ as the respective rates of change. Note that for the magnetic field, this is opposite from the convention set in the NRL Plasma Formulary, where the different components are being taken with respect to the direction of the magnetic field itself. We will denote $\bar{x}$ and $x$ as downstream and upstream variables, respectively. We will also use the notation $[\cdot]_1^2$ to denote the difference between the downstream and upstream quantities, for brevity.

The mass equation is

$$\frac{\partial\rho}{\partial t} + \frac{\partial}{\partial n}(\rho u_\perp) + \frac{\partial}{\partial s}(\rho u_\parallel) = 0.$$

As with the hydrodynamic shocks, we integrate the mass equation using a Gaussian pillbox at the shock

$$A\int_{-\epsilon}^{\epsilon} \mathrm{d}n\left(\frac{\partial\rho}{\partial t} + \frac{\partial}{\partial n}(\rho u_\perp) + \frac{\partial}{\partial s}(\rho u_\parallel)\right).$$

In the limit that $\epsilon \to 0$, the first and third terms vanish and we have $[\rho u_\perp]_1^2 = 0$.

The momentum equations are

$$\frac{\partial}{\partial t}(\rho u_\perp) + \frac{\partial}{\partial n}\left(\rho u_\perp^2 + P + \frac{B_\parallel^2 - B_\perp^2}{8\pi}\right) + \frac{\partial}{\partial s}\left(\rho u_\parallel u_\perp - \frac{B_\parallel B_\perp}{4\pi}\right) = 0$$

$$\frac{\partial}{\partial t}(\rho u_\parallel) + \frac{\partial}{\partial n}\left(\rho u_\perp u_\parallel - \frac{B_\perp B_\parallel}{4\pi}\right) + \frac{\partial}{\partial s}\left(\rho_\parallel^2 + P + \frac{B_\perp^2 - B_\parallel^2}{8\pi}\right) = 0$$

which, through a similar process, yield

$$\left[\rho u_\perp^2 + P + \frac{B_\parallel^2 - B_\perp^2}{8\pi}\right]_1^2 = 0$$

$$\left[\rho u_\perp u_\parallel - \frac{B_\perp B_\parallel}{4\pi}\right]_1^2 = 0.$$

The energy equation is

$$\frac{\partial E}{\partial t} + \frac{\partial}{\partial n}\left[u_\perp\left(E + P + \frac{B_\perp^2 + B_\parallel^2}{8\pi}\right) - \frac{B_\perp(\mathbf{u}\cdot\mathbf{B})}{4\pi}\right] + \frac{\partial}{\partial s}\left[u_\parallel\left(E + P + \frac{B_\perp^2 + B_\parallel^2}{8\pi}\right) - \frac{B_\parallel(\mathbf{u}\cdot\mathbf{B})}{4\pi}\right]$$

which yields

$$\left[u_\perp\left(E+P+\frac{B_\perp^2+B_\parallel^2}{8\pi}\right)-\frac{B_\perp\big(u_\perp B_\perp+u_\parallel B_\parallel\big)}{4\pi}\right]_1^2=0.$$

It will be more useful to write this in terms of primitive variables. The left side is then

$$\frac{\gamma}{\gamma-1}\,Pu_\perp+\frac{1}{2}\rho u_\perp\Big(u_\perp^2+u_\parallel^2\Big)-\frac{B_\parallel}{4\pi}\big(B_\perp u_\parallel-B_\parallel u_\perp\big).$$

The induction equations are

$$\begin{aligned}\frac{\partial B_\perp}{\partial t}+\frac{\partial}{\partial s}\big(B_\perp u_\parallel-B_\parallel u_\perp\big)&=0\\ \frac{\partial B_\parallel}{\partial t}+\frac{\partial}{\partial n}\big(B_\parallel u_\perp-B_\perp u_\parallel\big)&=0\end{aligned}$$

so it follows that $\big[B_\perp u_\parallel-B_\parallel u_\perp\big]_1^2=0$.

The magnetic field satisfies a divergence-free condition

$$\frac{\partial B_\perp}{\partial n}+\frac{\partial B_\parallel}{\partial s}=0$$

so $[B_\perp]_1^2=0$. This condition can be used to simplify some of the previous results. Performing these simplifications on the momentum and energy equations, we collect all six equations into

$$\begin{aligned}[\rho u_\perp]_1^2&=0\\ \left[\rho u_\perp^2+P+\frac{B_\parallel^2}{8\pi}\right]_1^2&=0\\ \left[\rho u_\perp u_\parallel-\frac{B_\perp B_\parallel}{4\pi}\right]_1^2&=0\\ \left[\frac{\gamma}{\gamma-1}\,Pu_\perp+\frac{1}{2}\rho u_\perp\Big(u_\perp^2+u_\parallel^2\Big)-\frac{B_\parallel}{4\pi}\big(B_\perp u_\parallel-B_\parallel u_\perp\big)\right]_1^2&=0\\ \big[B_\perp u_\parallel-B_\parallel u_\perp\big]_1^2&=0\\ [B_\perp]_1^2&=0.\end{aligned}$$

### 4.1 Special cases

The general behavior of MHD shocks is very complicated; special cases can considerably reduce the algebra involved.

The parallel shock is when the flow velocity and magnetic field are both normal to the shock front: $u_\parallel=B_\parallel=0$. Then the jump conditions reduce to those in the hydrodynamic case, and the magnetic field does not affect the qualitative properties of the shock. Denoting $M_s=u_\perp/v_s$ as the sonic Mach number,

$$\frac{\bar\rho}{\rho}=\frac{u_\perp}{\bar u_\perp}=\frac{(\gamma+1)M_s^2}{(\gamma-1)M_s^2+2},\qquad\frac{\bar B_\perp}{B_\perp}=1,\quad\text{and}\quad\frac{\bar P}{P}=1+\frac{2\gamma}{\gamma+1}\big(M_s^2-1\big).$$

The perpendicular case is when the flow velocity is normal to the magnetic field: $u_\parallel = B_\perp = 0$. In this case, let $r$ be

$$r = \frac{\bar{\rho}}{\rho} = \frac{u_\perp}{\bar{u}_\perp} = \frac{\bar{B}_\parallel}{B_\parallel}.$$

Substitution into the jump conditions yields a cubic in $r$. We verified that $r = 1$ is a trivial solution of the cubic, so the equation for $r$ reduces to a quadratic of the form

$$2(2-\gamma)r^2 + \gamma\big(2(1+\beta) + (\gamma-1)\beta M_s^2\big)r - \gamma(\gamma+1)\beta M_s^2 = 0$$

where $\beta = P/(B_\parallel^2/8\pi)$ is the plasma beta parameter. The product of the two roots satisfy

$$r_+ r_- = -\frac{\gamma(\gamma+1)\beta M_s^2}{2(2-\gamma)}.$$

Since $\gamma < 2$, one of the roots must be negative. But $r = \bar{\rho}/\rho > 0$, so we conclude that only $r_+$ is physical. Meanwhile, the rise in pressure is

$$\frac{\bar{P}}{P} = r + \frac{\gamma-1}{2}M_s^2\left(r - \frac{1}{r}\right) + \frac{\gamma-1}{\gamma}\frac{2}{\beta}r(1-r).$$

## 5 Implementation of the ideal MHD equations

We implemented a solver for the ideal MHD equations in 1D and 2D on a Cartesian grid from scratch.[†] Following the literature, we ignore the constants of $4\pi$ (equivalently, from SI units, $\mu_0 = 1$). We chose to implement this project in Julia [1] because of its high-level nature coupled with its performance. One can program high-level constructs in Julia as with other high-level, dynamic languages like Python, but switch over to a C-like style in performance-intensive lines. This allows us to benefit from the dynamicism and interactivity of the language without sacrificing performance, as one would in Python. Programming in a C-like style emphasizes memory management – it is expensive to allocate memory in the main loop, so preallocation and inplace updating is very important to prevent an excessive use of the garbage collector.

The CFL condition was calculated by using the maximum velocity of the system, which is set by the sum of the flow velocity $u$ and the fast magnetosonic speed $v_f$.

The spatial discretization was done using the 5th-order WENO finite-difference scheme with the Lax-Friedrichs flux splitting procedure [2, 3]. To ensure robustness of the numerical scheme, the numerical fluxes were calculated in local characteristic fields. The nonlinear weights as specified by Yamaleev and Carpenter [4] were used in the scheme and their calculation is, to our understanding, the bottleneck in the code. The time discretization was done using the total variation diminishing (TVD) 3rd-order Runge-Kutta method.

We implemented the AdaWENO scheme as proposed by Peng et al. [5] as a proof of concept extending its use beyond the Euler equations. The smoothness function

$$G_\pm = \rho + E \pm \alpha\rho\|\mathbf{u}\|$$

was used, where $\alpha$ is the Lax-Friedrichs parameter taken to be the largest speed on the grid. However, numerical oscillations were still present in this highly nonlinear system of PDEs. The specification of the smoothness function is problematic because it is empirically determined from

[†]https://github.com/Ininterrompue/weno

where discontinuities are located on the grid (e.g. if $E$ is discontinuous somewhere, then so is $G_\pm$). Therefore, we reverted to the characteristic reconstruction from before.

The eigensystem of (3) is treated as described in [3], and we do not repeat it here for brevity. However, we point out a typo in one of the left eigenvectors. The correct $L_{1,7}$ is

$$L_{1,7}^T = \frac{1}{2a^2}\begin{pmatrix} \gamma_1\alpha_f u^2 \pm \Gamma_f \\ (1-\gamma)\alpha_f u_x \mp \alpha_f c_f \\ (1-\gamma)\alpha_f u_y \pm c_s\alpha_s\beta_y \operatorname{sgn}(B_x) \\ (1-\gamma)\alpha_f u_z \pm c_s\alpha_s\beta_z \operatorname{sgn}(B_x) \\ (1-\gamma)\alpha_f B_y + \sqrt{\rho}\, a\alpha_s\beta_y \\ (1-\gamma)\alpha_f B_z - \sqrt{\rho}\, a\alpha_s\beta_z \\ (\gamma-1)\alpha_f \end{pmatrix}$$

with the correction to the typo highlighted in red (should be plus, not minus). Note that the vector has 7 elements because it refers to the 1D system. Another typo is when the authors discuss the "swap matrix," which relates the eigensystem of the $y$ flux vector $\mathbf{F}_y$ with the $x$ flux vector $\mathbf{F}_x$ like $\mathbf{F}_y = S\mathbf{F}_x(S\mathbf{Q})$, where $\mathbf{Q} = (\rho, \rho\mathbf{u}, E, \mathbf{B})^T$ is the MHD state vector. $S$ is correctly defined to be the matrix $S_{11} = S_{23} = S_{32} = S_{44} = S_{56} = S_{65} = S_{77} = S_{88} = 1$, with the other elements set to 0; in their paper, they forgot the nonvanishing diagonal elements. Applied to the eigensystems $R_{x,y}$ and $L_{x,y}$, the variables $u_x \leftrightarrow u_y$ and $B_x \leftrightarrow B_y$ are swapped. Then columns $2 \leftrightarrow 3$ and $5 \leftrightarrow 6$ of $R_{x,y}$ are swapped. For $L_{x,y}$, it is the rows that are swapped.

The definition

$$\operatorname{sgn}(B) = \begin{cases} +1 & B \geq 0 \\ -1 & B < 0 \end{cases}$$

which assigns $\operatorname{sgn}(0) = 1$ is particularly important in ensuring that the eigenvectors are nonsingular. We find that subtle numerical errors like these often arise in the code. For example, the square root in (9) may become slightly negative by a very small amount due to numerical round-offs resulting from the subtractive cancellation. A more subtle example was the situation where floating-point errors from matrix inversions eventually accumulated and crashed the simulation before $t = 4$ when the left eigenvectors were initially found by inverting the matrix of right eigenvectors instead of directly hardcoding the left eigenvectors.

### 5.1 Divergence constraint

It is important in any MHD code to ensure the divergence-free constraint $\boldsymbol{\nabla} \cdot \mathbf{B} = 0$. Failure to do so will result in unphysical solutions and numerical instabilities, as has been shown in the literature [3]. Divergence corrections were done by separately evolving the vector potential. There are no divergence corrections needed in 1D. In 2D, a choice of gauge allows the equation to simplify to a scalar advection equation [6]

$$\frac{\partial A_z}{\partial t} + (\mathbf{u} \cdot \boldsymbol{\nabla}) A_z = 0. \tag{11}$$

Equation (11) is of the form of a Hamilton-Jacobi equation. However, the WENO scheme for the Hamilton-Jacobi equation is of a slightly different form since it is the derivative of the vector potential whose oscillations we want to minimize. Given the MHD state vector $\mathbf{Q}$ and vector potential $A_z$ with initial conditions $\mathbf{Q}(0)$ and $A_z(0)$, we write

$$\frac{\partial \mathbf{Q}}{\partial t} = \mathcal{L}(\mathbf{Q}), \quad \mathcal{L} = -\boldsymbol{\nabla} \cdot \mathsf{F}$$
$$\frac{\partial A_z}{\partial t} = \mathcal{H}(A_z, \mathbf{u}), \quad \mathcal{H} = -(\mathbf{u} \cdot \boldsymbol{\nabla}) A_z$$

as the dynamical equations. The procedure is then given as follows [6].

First, we discretize $\mathcal{L}$ and $\mathcal{H}$ using the WENO scheme. The operator $\mathcal{L}$ is discretized in the usual way. However, $\mathcal{H}$ is modified to be

$$\mathcal{H}(A_z, \mathbf{u}) = -u_x\left(\frac{\partial_x A_z^+ + \partial_x A_z^-}{2}\right) - u_y\left(\frac{\partial_y A_z^+ + \partial_y A_z^-}{2}\right) + \alpha_x\left(\frac{\partial_x A_z^+ - \partial_x A_z^-}{2}\right) + \alpha_y\left(\frac{\partial_y A_z^+ - \partial_y A_z^-}{2}\right)$$

where $A_z^\pm$ are the positive and negative parts of $A_z$ after flux splitting, $\alpha_x = \max|u_x|$ and $\alpha_y = \max|u_y|$, and the maximums are taken across the global stencil. Of note is that we identify $\partial_x A_z^\pm$ and $\partial_y A_z^\pm$ with $\hat{f}_{i+1/2}^{\mp}$ to correctly calculate the nonlinear weights.

Second, we evolve $\mathbf{Q}$ and $A_z$ in time. We use the usual 3rd-order TVD Runge-Kutta method as before. We obtain a new $\mathbf{Q}^*$, which contains a magnetic field $\mathbf{B}^*$ that in general does not satisfy $\boldsymbol{\nabla} \cdot \mathbf{B}^* = 0$, as well as an energy $E^*$.

Third, we replace $\mathbf{B}^*$ by a discretized curl of $A_z$. In other words,

$$\begin{pmatrix} B_x^{n+1} \\ B_y^{n+1} \end{pmatrix} = \begin{pmatrix} +\partial_y A_z \\ -\partial_x A_z \end{pmatrix}.$$

The derivatives on the right are discretized using 4th-order central differencing.

Finally, we conserve the total energy. This means that we do not do anything to the calculated energy: $E^{n+1} = E^*$. Another option is to conserve the thermal pressure

$$E^{n+1} = E^* + \frac{\left\|\mathbf{B}^{n+1}\right\|^2 - \|\mathbf{B}^*\|^2}{2}$$

which may help in low $\beta$ plasmas to prevent the pressure from becoming negative, but this comes at the cost of conservation of energy.

It is important to note that in 2D, this correction only changes $B_x$ and $B_y$. $B_z$ can be left unchanged because there is no $z$ derivative, so $B_z$ does not contribute to the $\boldsymbol{\nabla} \cdot \mathbf{B} = 0$ condition.

### 5.2 Orszag-Tang vortex

The Orszag-Tang vortex is a popular 2D test for MHD. This test was done in our code because the boundary conditions were simple to implement so that efforts can be focused on the robustness of the numerical scheme of accurately capturing shocks and discontinuities. The vortex develops complex nonlinearities leading to turbulence and highlights shock-shock interactions.

The initial conditions are given as $\rho = \gamma^2$, $P = \gamma$, $u_x = -\sin y$, $u_y = \sin x$, $B_x = -\sin y$, $B_y = \sin 2x$, and $A_z = \frac{1}{2}\cos 2x + \cos y$. The grid is defined on $[0, 2\pi] \times [0, 2\pi]$. Our results show that the features become sharper in resolution as the grid size increases. Qualitatively, the contours agree with others in the literature [7]. Testing also confirms that the magnitude of $\boldsymbol{\nabla} \cdot \mathbf{B}$ never exceeds $10^{-13}$ anywhere on a $128 \times 128$ grid and never exceeds $10^{-12}$ on a $256 \times 256$ grid, both conditions holding for times up to the maximum time of simulation $t_{\max} = 4$. When the divergence corrections are not applied, we found that unphysical monopoles accumulate on the edge of the grid.

### 5.3 Linear wave test

The linear wave test is intended to demonstrate that the solution to the full nonlinear equations, with initial conditions of a small perturbation, can be reduced down to the linear (analytical) solution – plane waves. The perturbed quantities can be written in terms of $\mathbf{u}_1$ as

$$\rho_1 = \frac{\mathbf{k} \cdot \mathbf{u}_1}{\omega}\rho_0, \qquad P_1 = v_s^2 \rho_1, \quad \text{and} \quad \mathbf{B}_1 = \frac{\mathbf{k}}{\omega} \times (\mathbf{B}_0 \times \mathbf{u}_1).$$

We note that it is equivalent to consider the eigenvectors of $\mathbf{u}_1$ in (5). We rederived these eigenvectors to be

$$\begin{pmatrix} 1 \\ 0 \\ 0 \end{pmatrix} \quad \text{and} \quad \begin{pmatrix} 0 \\ \dfrac{v_s^2 k_\parallel^2}{\omega_{f,s}^2} - 1 \\ -\dfrac{v_s^2 k_\perp k_\parallel}{\omega_{f,s}^2} \end{pmatrix}$$

for the Alfvén and magnetosonic modes, respectively. We let $A_A$ and $A_{f,s}$ denote the amplitudes of these modes, with units of velocity.

To better show the effects of these waves in the code, we make a cyclic permutation of the coordinates, sending $y \to z$, $z \to x$, and $x \to y$. For an Alfvén wave with wavelength $\lambda = 1$, the primitive variables are then $\rho = \rho_0$, $P = P_0$, and

$$\begin{aligned} \mathbf{u} &= A_A \cos\left(2\pi(x - v_A t)\right)\hat{\mathbf{y}} \\ \mathbf{B} &= B_0\hat{\mathbf{x}} + \left(-\frac{A_A}{v_A}B_0\right)\cos\left(2\pi(x - v_A t)\right)\hat{\mathbf{y}} \end{aligned}$$

with vector potential

$$A_z = B_0 y + \frac{A_A}{v_A}\frac{B_0}{2\pi}\sin\left(2\pi(x - v_A t)\right).$$

These quantities are defined on the grid $[-1, 1] \times [-1, 1]$. The oscillatory parts are found by taking the real part of the complex exponential. The reduction to the linear regime is valid for $A_A t \ll \lambda$.

Since $A_z$ is linearly increasing with $y$, we must make a modification of the boundary conditions in that direction. We note that $A_z$ can be decomposed into a $y$-periodic $A_z^*$ and nonperiodic part, so that $A_z = B_0 y + A_z^*$. Let us assume that we are using one-based indexing and one ghost point for simplicity. Let `Az[end]` and `Az[1]` be the upper and lower ghost points corresponding to the largest and smallest value of $y$, respectively. Then it follows that since $\texttt{Az[end]}^* = \texttt{Az[2]}^*$ and $\texttt{Az[1]}^* = \texttt{Az[end-1]}^*$,

$$\begin{aligned} \texttt{Az[end]} &= \texttt{Az[2]} + \texttt{B0(y[end] - y[2])} \\ \texttt{Az[1]} &= \texttt{Az[end-1]} + \texttt{B0(y[1] - y[end-1])}. \end{aligned}$$

In Julia, it is very easy to modify the boundary conditions like this. We define a `SemiPeriodic` type which is a subtype of the abstract `BoundaryCondition` type. The only difference in implementation from the `Periodic` type (also a subtype of `BoundaryCondition`) is the behavior of $A_z$, so once we equate the boundary conditions for the primitive and conserved variables (omitting the other arguments for brevity)

```
boundaryconditions!(bctype::SemiPeriodic) = boundaryconditions!(Periodic())
```

and define the boundary conditions for $A_z$, the relevant function calls can be used in the high level loop once `SemiPeriodic` is specified.[†] This is an example of multiple dispatch in Julia.

If we denote the respective perturbations of the flow velocity and magnetic field by $\mathbf{u}_1$ and $\mathbf{B}_1$, then we see that

$$\mathbf{B}_1(t) = -\frac{\mathbf{u}_1(t)}{v_A}B_0, \tag{12}$$

[†]The exclamation point in the function is a language convention which denotes that the arguments are to be updated inplace. Omitted above are the system parameters and the MHD state vector.

a relation which was noted in [8]. However, the aforementioned reference mentions that (12) also applies for arbitrary amplitudes for all time, a condition that failed in the code because our Alfvén waves are linearly polarized. When we substitute back the perturbations into the full nonlinear equations, we pick up a nonvanishing magnetic pressure contribution. This quickly generates undesired magnetosonic waves in our simulation. Circularly polarized Alfvén waves, however, are a known solution to the fully nonlinear ideal MHD equations. Its implementation should reproduce the known relation (12).

## 6 Discussion

One of the disadvantages of the implemented numerical scheme is its performance in low $\beta$ plasmas because the calculation of the pressure

$$P = (\gamma - 1)\left(E - \frac{1}{2}\rho u^2 - \frac{B^2}{8\pi}\right)$$

after each time step involves the subtraction of two large numbers ($E$ and $B^2$). Huba [9] noted that the adiabatic pressure equation can be used in lieu of the energy equation, though the Rankine-Hugoniot jump conditions will not automatically be satisfied. Christlieb et al. [7] has recently proposed a method which is able to preserve the positivity of the mass density and pressure. Its reproduction is a possible future avenue for ensuring the robustness of the code.

## References


1. Bezanson, J., Edelman, A., Karpinski, S. & Shah, V. B. Julia: A Fresh Approach to Numerical Computing. *SIAM Review* **59,** 65–98 (2017).
2. Jiang, G. S. & Shu, C. W. Efficient Implementation of Weighted ENO Schemes. *J. Comput. Phys.* **126,** 202–228 (1996).
3. Jiang, G. S. & Wu, C. C. A High-Order WENO Finite Difference Scheme for the Equations of Ideal Magnetohydrodynamics. *J. Comput. Phys.* **150,** 561–594 (1999).
4. Yamaleev, N. K. & Carpenter, M. H. A Systematic Methodology for Constructing High-Order Energy Stable WENO Schemes. *J. Comput. Phys.* **228,** 4248–4272 (2009).
5. Peng, J., Zhai, C., Ni, G., Yong, H. & Shen, Y. An Adaptive Characteristic-wise Reconstruction WENO-Z Scheme for Gas Dynamic Euler Equations. *Comput. Fluids* **179,** 34–51 (2019).
6. Christlieb, A. J., Rossmanith, J. A. & Tang, Q. Finite Difference Weighted Essentially Non-Oscillatory Schemes with Constrained Transport for Ideal Magnetohydrodynamics. *J. Comput. Phys.* **268,** 302–325 (2014).
7. Christlieb, A. J., Feng, X., Seal, D. C. & Tang, Q. A High-Order Positivity-Preserving Single-Stage Single-Step Method for the Ideal Magnetohydrodynamic Equations. *J. Comput. Phys.* **316,** 218–242 (2016).
8. Sridhar, S. & Goldreich, P. Toward a Theory of Interstellar Turbulence. I. Weak Alfvenic Turbulence. *Astrophys. J.* **432,** 612–621 (1994).
9. Huba, J. Numerical Methods: Ideal and Hall MHD. *Proceedings of ISSS* **7,** 26–31 (2005).

## Appendix

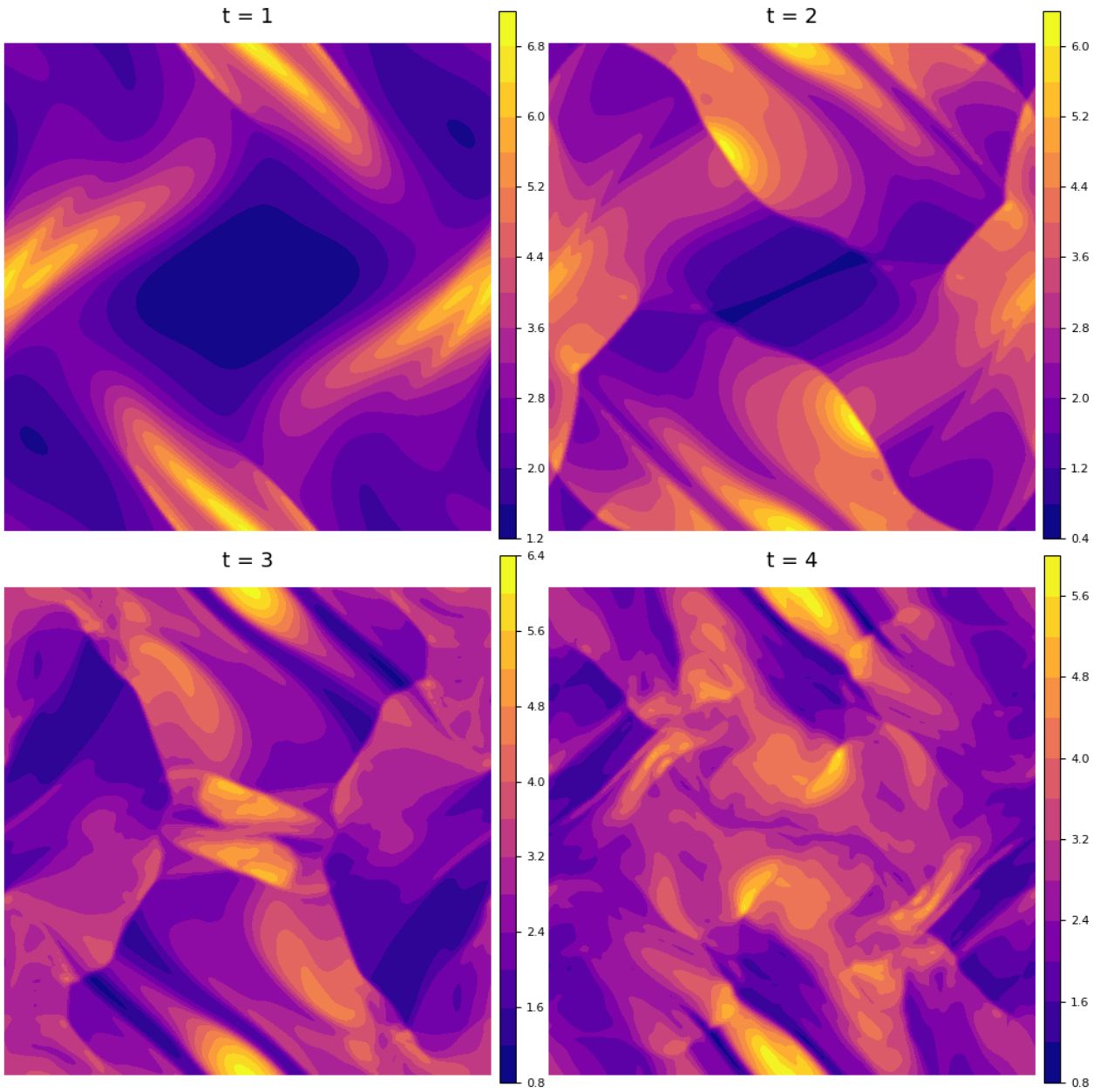


Figure 1: Mass density $\rho$ of the Orszag-Tang vortex at snapshots $t = 1$ to $t = 4$.

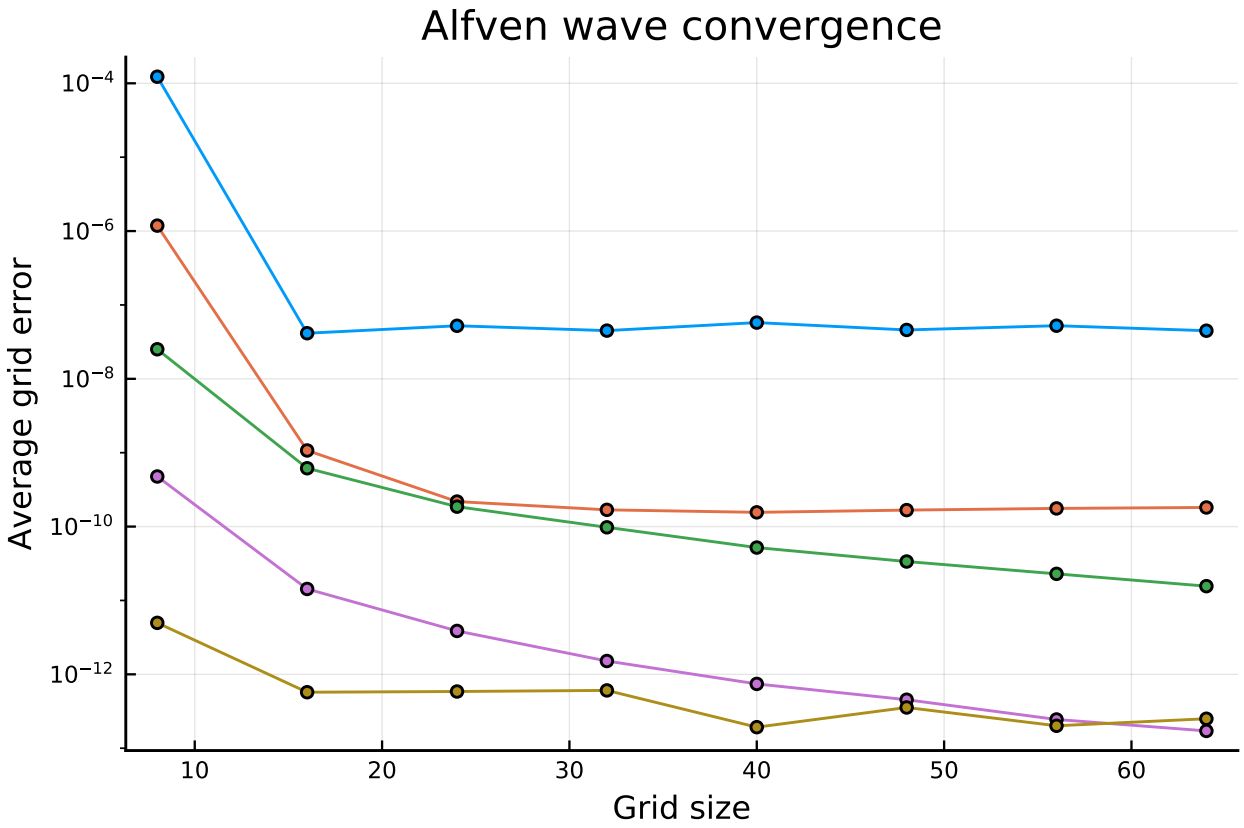


Figure 2: Convergence of the linear wave test. Shown are Alfvén wave perturbations of amplitudes $A_A = 10^{-1}$ to $10^{-5}$. Notice that $A_A = 10^{-1}$ and $10^{-2}$ corresponding to the blue and orange lines are not decreasing after a certain number of grid points because the perturbations are large enough for nonlinear effects to become nonnegligible. The convergence stops between $10^{-12}$ and $10^{-13}$ when numerical errors resulting from the discretization scheme start to dominate.

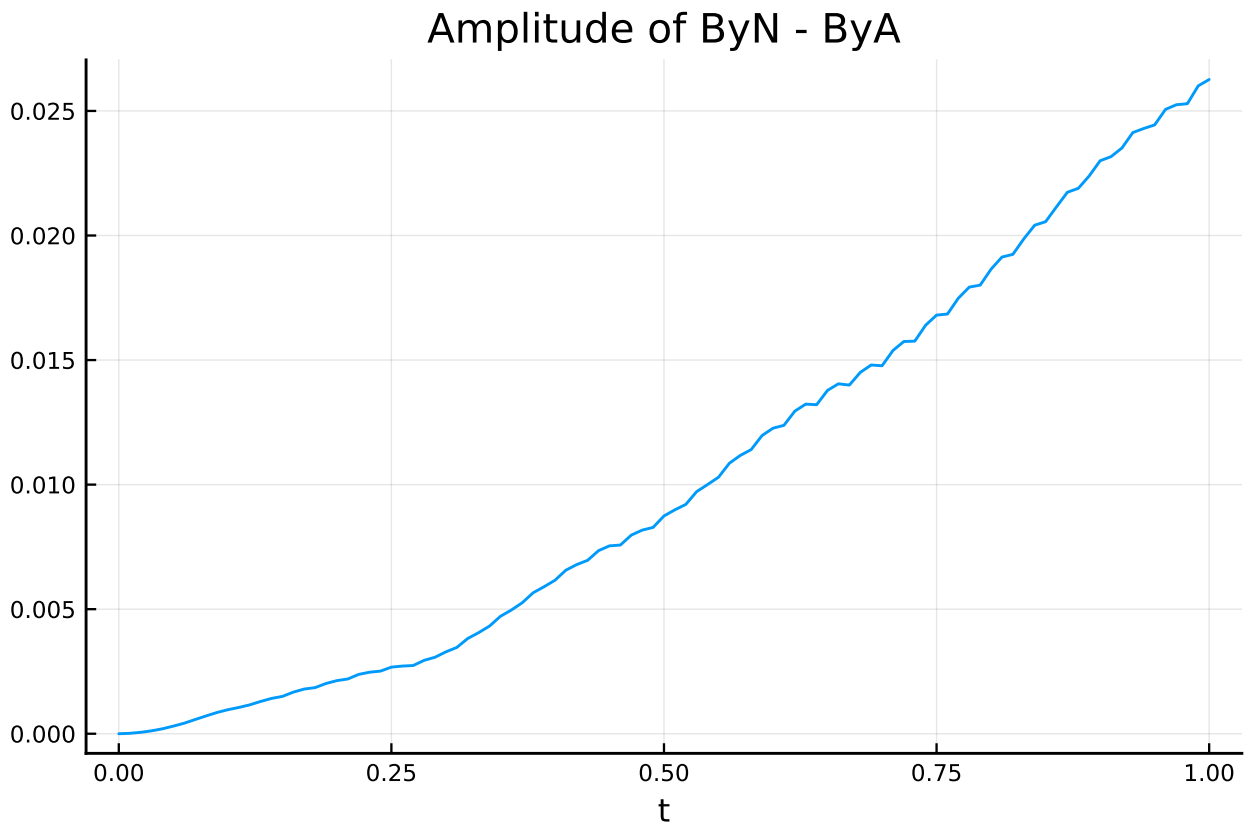


Figure 3: Maximum absolute difference between the amplitude of the numerical solution with the amplitude of the analytical solution at $A_A = 0.2$. As demonstrated in Figure 2, this amplitude is large enough for nonlinear effects to take hold. The nonlinearity is expected to grow exponentially until a certain time, after which nonlinear effects dominate. We do not see that – instead, the amplitude seems to increase linearly with time. Perturbing the system with a circularly polarized Alfvén wave should produce more accurate results since, as mentioned before, there is a nonvanishing magnetic pressure with linearly polarized waves which immediately generates undesired magnetosonic waves. This magnetic pressure vanishes with a circularly polarized wave.